The geometry of decision-making

Vivek Hari Sridhar[a,b,c,1], Liang Li[a,b,c,1], Dan Gorbonos[a,b,c], Máté Nagy[a,b,c,d,e,f], Bianca R. Schell[g], Timothy Sorochkin[h,i], Nir S. Gov[i] and Iain D. Couzin[a,b,c,1]

[a]Department of Collective Behaviour, Max Planck Institute of Animal Behavior, Konstanz, 78464 Konstanz, Germany

[b]Centre for the Advanced Study of Collective Behaviour, University of Konstanz, 78464 Konstanz, Germany

[c]Department of Biology, University of Konstanz, 78464 Konstanz, Germany

[d]MTA-ELTE Statistical and Biological Physics Research Group, Hungarian Academy of Sciences, 1117, Budapest, Hungary

[e]MTA-ELTE 'Lendület' Collective Behaviour Research Group, Hungarian Academy of Sciences, 1117, Budapest, Hungary

[f]Department of Biological Physics, Eötvös Loránd University, 1117, Budapest, Hungary

[g]Department of Chemistry, University of Konstanz, 78464 Konstanz, Germany

[h]Department of Physics & Astronomy, University of Waterloo, Waterloo, ON N2L 3G1, Canada

[i]Department of Chemical and Biological Physics, Weizmann Institute of Science, Rehovot 76100, Israel

Choosing among spatially-distributed options is a central challenge for animals, from deciding among alternative potential food sources or refuges, to choosing with whom to associate. Using an integrated theoretical and experimental approach (employing immersive virtual reality), we consider the interplay between movement and vectorial integration during decision-making regarding two, or more, options in space. In computational models of this process we reveal the occurrence of spontaneous and abrupt "critical" transitions (associated with specific geometrical relationships) whereby organisms spontaneously switch from averaging vectorial information among, to suddenly excluding one, among the remaining options. This bifurcation process repeats until only one option—the one ultimately selected—remains. Thus we predict that the

brain repeatedly breaks multi-choice decisions into a series of binary decisions in space-time. Experiments with fruit flies, desert locusts, and larval zebrafish reveal that they exhibit these same bifurcations, demonstrating that across taxa and ecological context, there exist fundamental geometric principles that are essential to explain how, and why, animals move the way they do.

Animals constantly face the need to make decisions, and many such decisions require choosing among multiple spatially-distributed options. Despite this, most studies have focused on the outcome of decisions (1–3) (i.e. which option among alternatives is chosen), as well as the time taken to make decisions (4–6), but seldom on the movement of animals throughout the decision-making process. Motion is, however, crucial in terms of how space is represented by organisms during spatial decision-making; the brains of a wide range of species, from insects (7, 8) to vertebrates (9, 10), have been shown to represent egocentric spatial relationships, such as the position of desired targets, via explicit vectorial representation (11, 12). Such neuronal representations must, and do, change as animals move through space. Thus, while the movement of an animal may, initially, appear to simply be a readout of the decision made by the brain—and consequently not particularly informative—this view overlooks important dynamical properties introduced into the decision-making process that result from the inevitable time-varying geometrical relationships between an organism and spatially-distributed options (i.e. potential 'targets' in space).

Due to a dearth of existing studies, and with the objective to develop the necessary foundational understanding of the 'geometry' of decision-making, we focus here—first theoretically and then experimentally—on the consequences of the recursive interplay between movement and (collective) vectorial integration in the brain during relatively simple spatial decisions. We

52 employ immersive virtual reality to investigate decision-making regarding multiple (two or
53 more) options in both invertebrate (the fruit fly *Drosophila melanogaster*, and desert locust
54 *Schistocerca gregaria*) and vertebrate (larval zebrafish *Danio rerio*) models. Doing so allows
55 us to reveal the emergence of geometric principles that transcend the study organism and the
56 decision-making context, and thus are expected to be broadly relevant across taxa. In support
57 of this finding we also explore how these principles extend to collective decision-making in
58 mobile animal groups, allowing us to gain insights across three scales of biological
59 organisation, from neural dynamics, to both individual and collective decision-making.
60

61 ## Modelling decision-making on the move

62 Congruent with neurobiological studies of the invertebrate and vertebrate brain, we consider
63 organisms to have an egocentric vectorial representation of spatial options (11–13). We then
64 consider the collective dynamics of vector integration in the brain assuming there exists
65 reinforcement (excitation/positive feedback) among neural ensembles that have similar
66 directional representations (goal vectors), and global inhibition and/or negative feedback (both
67 produce broadly similar results, see SI Appendix and Fig. S1) among neural ensembles that
68 differ in vectorial representation. This captures, in a simple mathematical formulation, the
69 essence of both explicit ring-attractor networks (as found in insects (7)), and computation
70 among competing neural groups (as in the mammalian brain (14)). The animal's relative
71 preference for a target is given by activity of neurons that encode direction to that target relative
72 to activity of neurons that encode direction to other targets, and the angular sensitivity of the
73 neural representations (angular difference at which excitation no longer occurs) is specified by
74 a neural tuning parameter, ν. The network then computes a unique 'consensus' vector ('activity
75 bump') that, along with some angular noise, represents the animal's desired direction of
76 movement (Fig. S2). This is then translated into motor output (see SI Appendix for model

details \cite{pinkoviezky_collective_2018}). Stochasticity in neural dynamics is implemented here as the neural noise parameter, T.

While capturing known, generic features of neural integration, our model is deliberately minimal. This serves multiple purposes: firstly, following principles of maximum parsimony we seek to find a simple model that can both predict and explain, the observed phenomena; secondly, we aim to reveal general principles and thus consider features that are known to be valid across organisms irrespective of inevitable difference in structural organization of the brain; thirdly, it provides a convenient means to implement neural noise, and can be mapped to the class of neural ring-attractor models widely-used in neuroscience (15–18) (see SI Appendix for details). In addition, our results are shown to be extremely robust to model assumptions, suggesting that it provides an appropriate low-level description of essential system properties.

Deciding between two options

Beginning with the simplest case, we consider the feedback between motion and internal vectorial-computation when an animal is presented with two equally-attractive, but spatially-discrete, options. In this case the activity of neurons encoding option 1, N_1 will be equal to those encoding option 2, N_2 (Fig. 1A). Our model predicts that an animal moving, from a relatively distant location, towards the two targets, will spontaneously compute the average directional preference, resulting in corresponding motion in a direction oriented between the two targets. As it approaches the targets, however, upon reaching a certain angular difference between the options, the internal network undergoes a sudden transition in which it spontaneously selects one, or the other, target (Fig. 1C). This results in an abrupt change in

trajectory, the animal being redirected towards the respective 'selected' target (Fig. 1C; see also Fig. S3A for the same phenomenon occurring for a wide range of starting positions).

Our model therefore predicts that despite the fact that the egocentric geometrical relationship between the animal and the targets changes continuously, upon approaching the targets, there exists a location whereby a further, very small, increase in angular difference between the targets will result in a sudden change in system (neural) dynamics, and consequently in motion, and thus decision-making. Such spatio-temporal dynamics do not occur if individuals were to simply integrate noisy vectorial information or choose their travel direction from a summed distribution of the location of targets in their sensory field (19), points we will return to later.

In numerical analysis of our model we find that irrespective of starting position, as the animal reaches the respective angle in space, it will relatively suddenly select one of the options (Fig. S3A). While the specific angular difference at which this phenomenon occurs is dependent on neural tuning, ν (Fig. S3C), and the starting configuration (due to an interplay between the two timescales involved—for movement and for neural consensus, see Fig. S3B), it is always present as long as the neural noise, T remains below a critical firing rate, T_c (although even for $T < T_c$, these bifurcations may be difficult to see for small values of ν due to inherent noise in real biological systems; see Fig. S4 for simulations where vectorial representations of targets include directional error).

To gain a deeper insight into the mechanism underlying the observed spatiotemporal dynamics, we constructed a mean-field approximation of our model (see SI Appendix) since this has the advantage of allowing us to conduct formal analyses of patterns realized in the simulated trajectories.

Geometric principles of decision-making

The mean-field analysis of our model shows that below a critical level of neural noise, animals will adopt the average among options as they approach the targets, until a critical phase transition upon which the system spontaneously switches to deciding among the options (Figs. 1B and S5A). Thus despite varying in its exact location (Fig. 1B), the sudden transition observed is an inevitable consequence of the system dynamics and will always occur.

Such sudden transitions correspond to 'bifurcations' in the mathematical study of dynamical systems. A bifurcation is said to occur when a smooth change in an external parameter, in this case perceived angular difference between the options, causes a sudden qualitative change in the system's behavior, here corresponding to a literal bifurcation (or branching) in physical space.

When dynamical systems undergo such a phase, or quasi-phase, transition they exhibit a remarkable universal property: close to the transition, at the "critical-point" or "tipping-point", the system spontaneously becomes extremely sensitive to very small perturbations (e.g. to small differences in preference between options (20, 21)). This is true of both physical (e.g. magnetic (22)) and biotic (e.g. cellular (23, 24)) systems undergoing a phase transition. Correspondingly, we find that below a critical level of neural noise, the mean-field model exhibits a sudden increase in susceptibility as the animal approaches the critical point, immediately prior to the decision being made (Fig. S5A). This will not occur in previously-considered models where an animal is assumed to choose its direction of travel based on the summed distribution of targets in its sensory field, also known as probability density function, or PDF, sum-based models (19). Thus, as animals approach targets we predict they will pass

151 through a window of space (corresponding to the critical angle for the respective geometry they
152 are experiencing) in which their brain spontaneously becomes capable of discriminating
153 between very small differences between options (e.g. a very small difference in neuronal
154 activity being in 'favor' of one option; see Fig. S3D and SI Appendix for details). This highly-
155 valuable property (for decision-making) is not built into the model, but is rather an emergent
156 property of the inherent collective dynamics.
157
158 In many real biological systems, including the ones we consider here, the (neural) system size
159 is typically not large enough to consider true phase transitions (which only occur for very large
160 systems, as per the mean-field approximation), but rather 'phase-transition-like', or 'quasi-
161 phase transition', behavior. Even though real biological systems are not necessarily close to the
162 infinite size limit of the mean-field approximation, we see very similar dynamics for both small
163 and large system sizes (Fig. S6).
164

165 Decision-making beyond two options

166 While the majority of decision-making studies consider only two options (due to both
167 theoretical and experimental tractability (14, 25, 26)), animals moving in real space frequently
168 encounter a greater number than this. Here we consider how animals will be expected to select
169 among three, or more, options (possible targets) in space. First we begin with three identical
170 options ($N_1 = N_2 = N_3$) since this gives us the clearest insight into the relationship between
171 motion and decision-making dynamics. Then we relax these assumptions and consider
172 differences between options (Fig. S3E) as well as a greater number of options (Fig. 2). Note
173 that we do not modify our model in any way prior to introducing these additional complexities.
174

Below T_c (see SI Appendix and Fig. S7 for considerations when $T > T_c$), we once again find that the direction in which the animal moves is a function of the angular difference between the targets. When relatively far from the targets, it moves in the average of these three directions. Upon reaching a critical angular threshold between the leftmost and rightmost option (from the animal's perspective), however, the neural system spontaneously eliminates one of them and the animal begins moving in the direction average between the two remaining options (Fig. 1D,E). It continues in this direction until a second critical angle is reached, and now the animal eliminates one of the two remaining options and moves towards the only remaining target (Figs. 1F and S5B). Thus we predict that the brain repeatedly breaks multi-choice decisions into a series of binary decisions in space-time. Such bifurcation dynamics are not captured in models of decision-making that do not include the required feedbacks, such as if individuals simply sum noisy vectors (or PDFs) to targets in their sensory field (19). For the case of three targets, vectors/votes to the leftmost option would tend to cancel those that favor the rightmost option, resulting in the selection of the central option, an issue we will return to later when considering collective animal behavior. Simulating a larger number of options (Fig. 2) and varying environmental geometries (Figs. S8 and S9) demonstrate the robustness of this mechanism in the face of environmental complexity and the more complex spatial dynamics that emerge as organisms undergo repeated bifurcations.

Experimental tests of our predictions

Since the decision-process is predicted to be sequential, and dependent on the geometry with respect to the targets from an egocentric perspective, it should be possible to visualize it directly from the trajectories taken by animals when making spatial decisions. In this respect, our theoretical studies make a key testable prediction: if neural groups within the decision-making ensemble exhibit relatively local excitation, and long-range/global inhibition, we should

observe bifurcations in the animals' trajectories as they choose among identical options; and that if animals face three (or more) such options, then the complex decision task should be broken down to a series of binary decisions.

Since the geometrical principles revealed above are expected to be both robust and generic, we use immersive virtual reality (27) (Fig. S10) to test our predictions by investigating both two- and three-choice decision-making in three evolutionarily highly-divergent brains under ecologically-relevant scenarios: fruit flies (*Drosophila melanogaster*) and desert locusts (*Schistocerca gregaria*) deciding which among multiple vertical objects to approach (e.g. to perch), and zebrafish (*Danio rerio*) choosing with which conspecific(s) to school.

Like many other insects (28–31), fruit flies (32) and desert locusts (33) exhibit a natural tendency to orient and move towards high-contrast vertical features (potential landing sites or indicators of vegetation) in their environment. We exploit this tendency, presenting multiple identical black pillars as targets in an otherwise white environment. We record trajectories of our focal animals (solitary flies or locusts) as they choose to move towards one of these pillars, thus obtaining a behavioral readout of the decision-making process (see SI Appendix for experimental details; Figs. S11 and S12 show raw trajectories of flies and locusts respectively).

As predicted by our theory (Fig. 1B,C), we find that, in the two-choice case, most flies and locusts that choose one of the presented targets initially move in the average of the egocentric target directions until a critical angular difference (Fig. S13), at which point they select (randomly) one, or the other, option and move towards it (randomization test where $y-$coordinates between trajectories were swapped showed that the bifurcation fit to our experimental data was highly significant; $p < 0.01$ for both flies and locusts; Figs. 1G and

S13). Here, we note that there may be multiple factors that affect the animals' direction of movement. For example, it could be that animals repeatedly switch between fixating on each of the two options before reaching the critical angular difference, following which it selects one. However, quantification of their heading relative to the targets, and to the average direction between the targets (Fig. S13), finds no evidence for this; instead, prior to the bifurcation, both flies and locusts exhibit a heading towards the average of the egocentric target directions. In the three-choice case, the animals' movements are also consistent with our theory; as predicted (Fig. 1E,F) they break the three-choice decision into two sequential binary decisions ($p < 10^{-4}$ for both flies and locusts; Fig. 1H). For both animals, the observed angle of bifurcation ($\sim 110°$ for flies and $\sim 90°$ for locusts) is much larger than their visual spatial resolution ($\sim 8°$ and $\sim 2°$ for flies (34) and locusts (35, 36), respectively). We note $\sim 30\%$ of animals in our experiments (both flies and locusts) did not exhibit the sequential bifurcations (see Figs. S11 and S12) described above, and instead moved directly towards one of the presented targets (Figs. S11 and S12). Such variability in response is expected in animals, and is consistent with recent work on the visual response of flies, which demonstrates a link between stochastic (non-heritable) variation in brain wiring within the visual system and strength of visual orientation response to a vertical stripe target (37). Furthermore, flies that experience high temperatures during development appear to exhibit a particularly strong orientation tendency, exhibiting the most direct paths to targets while flies that experience low developmental temperatures exhibit wandering paths to targets (38). In our model such differences can be accounted for by variation in directional tuning of the neural groups, with high directional tuning (low ν) being associated with a strong orientational response, and such individuals exhibiting direct tracks to targets from the outset (see Fig. S14).

A further, non-mutually exclusive, possibility, is that a subset of insects exhibit "handedness". For example, in (39), it was shown that approximately 25% of *Drosophila* were either strongly left-biased or right-biased when moving on a Y-maze, and that these consistent differences among flies were similarly non-heritable. This experimental design did not assess whether a further subset are biased to go directly forwards if offered three directional choices (such as could occur in a hypothetical Ψ maze). In such cases, it is certainly possible that these intrinsic directional biases break symmetry (Fig. S3D,E), resulting in directed paths to different targets.

We note that individuals predisposed to exhibit direct paths to targets would be expected to make faster, yet less accurate, decisions, a prediction we plan to test in future studies.

Our zebrafish experiments consider spatial decision-making in a social context. We present virtual conspecifics (see SI Appendix for methodological details) that move back-and-forth in the arena parallel to each other as targets (Figs. 3A and S15A) and behave (Fig. S16), and are responded to (Fig. S17), in the same way as real fish. Because they are social, the real fish respond to these virtual fish by tending to follow at a (relatively) fixed distance behind them (Fig. S15E). Our data are best represented within this moving frame of reference (the virtual fish; Fig. S15). Theoretically we predict that for two virtual fish we should see a single bifurcation, where the real fish will suddenly switch from averaging the target directions to deciding among them (i.e. swimming predominantly with one of the virtual fish), as a function of increasing the lateral distance, L, between the virtual fish (Figs. 3B and S18; see SI Appendix for details of model implementation). The existence of this bifurcation is clearly seen in our experiments (Fig. 3C). When considering three moving virtual conspecifics, the model predicts that real fish will spontaneously break the three-choice decision to two binary decisions, and a

comparison of the theoretical prediction and experimental results demonstrates this to be the case (c.f. Fig. 3E,F).

We also test predictions under conditions where there is an asymmetric geometry whereby two fish swim closer to each other than the central one does to the third fish (Fig. 4A). As predicted by our theory (Fig. 4B), the real fish tends to swim between the two closely-associated fish, or close to the third, more distant, fish (Fig. 4B). Note that, also as predicted, the real fish spends a similar amount of time in each of the two locations.

Although detailed models considering the specifics of each system would be expected to provide additional quantitative fits (at the expense of losing some degree of generality and analytical tractability), our results are broadly independent of the model implementation details. Thus, we find that the key predictions of our model are validated in fruit flies, desert locusts and larval zebrafish in distinct, yet ecologically relevant contexts.

Model features that determine network behavior

There are key features that are essential to produce the bifurcation patterns observed in our data i.e. for any decision-making system to break multi-choice decisions to a series of binary decisions.

- Feedback processes that provide the system directional persistence, and drive such bifurcations, are crucial to exhibit the observed spatio-temporal dynamics. In the neural system, this is present in the form of local excitation and long-range/global inhibition (7, 16, 17). However, as shown in our model of collective animal behavior below, we expect that similar dynamics will be observed if the necessary feedbacks are also

incorporated into other models of decision-making, such as to PDF-sum-based models, for example (19).

- Observing similar decision dynamics requires a recursive (embodied) interplay between neural dynamics, and motion in continuous space. Here, the animal's geometrical relationship with the targets changes as it moves through physical space. Since neural interactions depend on this changing relationship, space provides a continuous variable by which the individual traverses the time-varying landscape of neural firing rates.

These essential features, along with the observed animal trajectories in the two-choice context, are reminiscent of collective decision-making in animal groups (models (40–44), fish schools (45), bird flocks (46) and baboon troops (25)). Below, we consider an established model of collective decision-making (40) to draw links between these two scales of biological organization—decision-making in the brain, and decision-making in animal groups.

A link to collective decision-making

In order to draw a link between individual decision-making and collective decision-making in animal groups, we consider an animal group with equal number of individuals exhibiting preference for each target (see SI Appendix for methodological details). A long-standing approach in the study of animal collectives is to consider them integrating vectorial information from neighbors (47, 48), and there are a great number of publications of such “flocking”, “schooling” or “herding” behaviors (47–49). Individuals within groups may also have preferences to reconcile this local vector-averaging with goal-oriented behavior, such as a desired direction of travel (40, 45), and such models have made effective predictions regarding how the number of individuals with a common desired direction of travel influences the accuracy of group motion towards targets (25) and how the weighting of the internal ‘goal-

oriented' vector representing the desired direction of travel, influences the capacity and accuracy for individuals to act as leaders and to influence the directon taken by the group as a whole (50).

We demonstrate here, however, that while ubiquitous, such models of collective animal behavior fail to account for the known capability for animal groups to make decisions among spatially discrete targets (see Fig. S19A,B). To do so, it is essential that the necessary feedbacks, as described above for collective decision-making among neurons, are incorporated. While these feedbacks are inherent to our neural model, they can also be included in other models in the form of social interactions, or in the animals' response to their environment (51).

For example, one way feedback can be introduced here is via ‘informed’ individuals (those with a desired direction of travel) associating with ‘uninformed’ or ‘unbiased' individuals (individuals that exhibit social interactions but have no specific desired direction of travel) (40, 45); ‘uninformed’ individuals are effectively recruitable by those with a desired direction of travel (providing local positive feedback), but are also in finite supply, creating what is effectively a competition among informed subsets that differ in their preferred direction of travel (a form of longer-range inhibition between informed subsets). However, because ‘uninformed' individuals tend to average the direction of all ‘informed' individuals that recruit them, we find that this type of feedback functions more as a social glue, and is only able to explain bifurcations when the group is choosing between two options. In a decision-making context with three options, this type of feedback, alone, results in the group almost always moving towards the central target (Fig. S19D).

A means of resolving this issue is for individuals to change the strength of their goal-orientedness as a function of their experienced travel direction; for example, individuals that find themselves consistently moving in a (group) direction that differs from their preferred target direction could weaken the strength of their preference over time (a form of forgetting/negative feedback, effectively resulting in long-range/global inhibition; and once this preference is lost, they will tend to spontaneously reinforce the majority-selected direction (45), a form of positive feedback). We find that this biologically-plausible mechanism (40) will allow individuals within the group to recover the capability to come to consensus even in the absence of uninformed individuals (Fig. 5), and for a greater number of options than two (Fig. 5B).

Despite considerable differences in details between this model and that of neural dynamics described above, with the former involving individual components that change neighbor-relationships over time and where inhibition emerges from a different biological process, the predictions regarding motion during decision-making are extremely similar (c.f. Fig. 5 and Fig. 1 for a comparison between predictions for animal groups and neural groups, respectively). Thus, we find that similar principles may underlie spatial decision-making across multiple scales of biological organization. Furthermore by presenting social interactions in a decision-making context, our zebrafish experiments elucidate the neural basis of schooling allowing us to glean insights across three scales of biological organization—from neural dynamics to individual decisions, and from individual decisions to collective movement.

Conclusions

We demonstrate that, across taxa and contexts, explicitly considering the time-varying geometry during spatial decision-making provides new insights that are essential to understand

371 how, and why, animals move the way they do. The features revealed here are highly robust,
372 and we predict that they occur in decision-making processes across various scales of biological
373 organization, from individuals to animal collectives (see Figs. 5 and S19, and SI Appendix),
374 suggesting they are fundamental features of spatiotemporal computation.

375

376 ## References

377 1. C. E. J. Kennedy, J. A. Endler, S. L. Poynton, H. McMinn, Parasite load predicts mate
378 choice in guppies. *Behav Ecol Sociobiol* **21**, 291–295 (1987).

379 2. K. Summers, R. Symula, M. Clough, T. Cronin, Visual mate choice in poison frogs.
380 *Proceedings of the Royal Society of London. Series B: Biological Sciences* **266**, 2141–
381 2145 (1999).

382 3. E. Forsgren, Predation Risk Affects Mate Choice in a Gobiid Fish. *The American Naturalist*
383 **140**, 1041–1049 (1992).

384 4. R. Kiani, L. Corthell, M. N. Shadlen, Choice Certainty Is Informed by Both Evidence and
385 Decision Time. *Neuron* **84**, 1329–1342 (2014).

386 5. J. M. Beck, *et al.*, Probabilistic Population Codes for Bayesian Decision Making. *Neuron*
387 **60**, 1142–1152 (2008).

388 6. A. K. Churchland, R. Kiani, M. N. Shadlen, Decision-making with multiple alternatives.
389 *Nature Neuroscience* **11**, 693–702 (2008).

390 7. S. S. Kim, H. Rouault, S. Druckmann, V. Jayaraman, Ring attractor dynamics in the
391 Drosophila central brain. *Science* **356**, 849–853 (2017).

392 8. J. D. Seelig, V. Jayaraman, Neural dynamics for landmark orientation and angular path
393 integration. *Nature* **521**, 186–191 (2015).

394 9. J. S. Taube, R. U. Muller, J. B. Ranck, Head-direction cells recorded from the
395 postsubiculum in freely moving rats. II. Effects of environmental manipulations. *Journal*
396 *of Neuroscience* **10**, 436–447 (1990).

397 10. A. Finkelstein, *et al.*, Three-dimensional head-direction coding in the bat brain. *Nature*
398 **517**, 159–164 (2015).

399 11. A. Sarel, A. Finkelstein, L. Las, N. Ulanovsky, Vectorial representation of spatial goals in
400 the hippocampus of bats. *Science* **355**, 176–180 (2017).

401 12. Ø. A. Høydal, E. R. Skytøen, S. O. Andersson, M.-B. Moser, E. I. Moser, Object-vector
402 coding in the medial entorhinal cortex. *Nature* **568**, 400–404 (2019).

13. R. Wehner, B. Michel, P. Antonsen, Visual navigation in insects: coupling of egocentric and geocentric information. *Journal of Experimental Biology* **199**, 129–140 (1996).

14. A. Bahl, F. Engert, Neural circuits for evidence accumulation and decision making in larval zebrafish. *Nature Neuroscience* **23**, 94–102 (2020).

15. K. Zhang, Representation of spatial orientation by the intrinsic dynamics of the head-direction cell ensemble: a theory. *J. Neurosci.* **16**, 2112–2126 (1996).

16. X. Sun, M. Mangan, S. Yue, An Analysis of a Ring Attractor Model for Cue Integration in *Biomimetic and Biohybrid Systems*, Lecture Notes in Computer Science., V. Vouloutsi, *et al.*, Eds. (Springer International Publishing, 2018), pp. 459–470.

17. L. C. York, M. C. W. van Rossum, Recurrent networks with short term synaptic depression. *J Comput Neurosci* **27**, 607–620 (2009).

18. S. I. Wiener, J. S. Taube, *Head Direction Cells and the Neural Mechanisms of Spatial Orientation* (MIT Press, 2005).

19. B. Collignon, A. Séguret, J. Halloy, A stochastic vision-based model inspired by zebrafish collective behaviour in heterogeneous environments. *Royal Society Open Science* **3**, 150473 (2006).

20. L. Benedetti-Cecchi, L. Tamburello, E. Maggi, F. Bulleri, Experimental perturbations modify the performance of early warning indicators of regime shift. *Current Biology* **25**, 1867–1872 (2015).

21. A. Gelblum, *et al.*, Ant groups optimally amplify the effect of transiently informed individuals. *Nature Communications* **6** (2015).

22. B. M. McCoy, T. T. Wu, *The two-dimensional Ising model: second edition* (Courier Corporation, 2014).

23. J.-M. Choi, A. S. Holehouse, R. V. Pappu, Physical Principles Underlying the Complex Biology of Intracellular Phase Transitions. *Annual Review of Biophysics* **49**, 107–133 (2020).

24. A. A. Hyman, K. Simons, Beyond Oil and Water—Phase Transitions in Cells. *Science* **337**, 1047–1049 (2012).

25. A. Strandburg-Peshkin, D. R. Farine, I. D. Couzin, M. C. Crofoot, Shared decision-making drives collective movement in wild baboons. *Science* **348**, 1358–1361 (2015).

26. R. Ratcliff, P. L. Smith, S. D. Brown, G. McKoon, Diffusion Decision Model: Current Issues and History. *Trends in Cognitive Sciences* **20**, 260–281 (2016).

27. J. R. Stowers, *et al.*, Virtual reality for freely moving animals. *Nature Methods* **14**, 995–1002 (2017).

437 28. T. Poggio, W. Reichardt, A theory of the pattern induced flight orientation of the fly
438 Musca domestica. *Kybernetik* **12**, 185–203 (1973).

439 29. D. Varju, Stationary and dynamic responses during visual edge fixation by walking
440 insects. *Nature* **255**, 330–332 (1975).

441 30. W. Reichardt, T. Poggio, A theory of the pattern induced flight orientation of the fly
442 Musca domestica II. *Biological Cybernetics* **18**, 69–80 (1975).

443 31. P. K. Kaushik, M. Renz, S. B. Olsson, Characterizing long-range search behavior in Diptera
444 using complex 3D virtual environments. *PNAS* **117**, 12201–12207 (2020).

445 32. E. Horn, R. Wehner, The mechanism of visual pattern fixation in the walking fly,
446 Drosophila melanogaster. *Journal of Comparative Physiology A* **101**, 39–56 (1975).

447 33. G. K. Wallace, Some experiments on form perception in the nymphs of the desert locust,
448 Schistocerca gregaria forskål. *Journal of Experimental Biology* **35**, 765–775 (1958).

449 34. P. T. Gonzalez-Bellido, T. J. Wardill, M. Juusola, Compound eyes and retinal information
450 processing in miniature dipteran species match their specific ecological demands.
451 *Proceedings of the National Academy of Sciences* **108**, 4224–4229 (2011).

452 35. O. Faivre, M. Juusola, Visual coding in locust photoreceptors. *Plos One* **3**, e2173 (2008).

453 36. M. Wilson, Angular sensitivity of light and dark adapted locust retinula cells. *Journal of*
454 *Comparative Physiology* **97**, 323–328 (1975).

455 37. G. A. Linneweber, *et al.*, A neurodevelopmental origin of behavioral individuality in the
456 Drosophila visual system. *Science* **367**, 1112–1119 (2020).

457 38. F. R. Kiral, *et al.*, Variable brain wiring through scalable and relative synapse formation in
458 Drosophila. *bioRxiv* (2021) https:/doi.org/10.1101/2021.05.12.443860.

459 39. S. M. Buchanan, J. S. Kain, B. L. de Bivort, Neuronal control of locomotor handedness in
460 Drosophila. *PNAS* **112**, 6700–6705 (2015).

461 40. I. D. Couzin, J. Krause, N. R. Franks, S. A. Levin, Effective leadership and decision-making
462 in animal groups on the move. *Nature* **433**, 4 (2005).

463 41. B. Nabet, N. E. Leonard, I. D. Couzin, S. A. Levin, Dynamics of Decision Making in Animal
464 Group Motion. *J Nonlinear Sci* **19**, 399–435 (2009).

465 42. N. E. Leonard, *et al.*, Decision versus compromise for animal groups in motion.
466 *Proceedings of the National Academy of Sciences* **109**, 227–232 (2012).

467 43. R. Gray, A. Franci, V. Srivastava, N. E. Leonard, Multiagent Decision-Making Dynamics
468 Inspired by Honeybees. *IEEE Transactions on Control of Network Systems* **5**, 793–806
469 (2018).

44. A. Bizyaeva, A. Franci, N. E. Leonard, A General Model of Opinion Dynamics with Tunable Sensitivity. *arXiv:2009.04332 [cs, eess, math]* (2020) (July 26, 2021).

45. I. D. Couzin, *et al.*, Uninformed individuals promote democratic consensus in animal groups. *Science* **334**, 1578–1580 (2011).

46. D. Biro, D. J. T. Sumpter, J. Meade, T. Guilford, From compromise to leadership in pigeon homing. *Current Biology* **16**, 2123–2128 (2006).

47. I. D. Couzin, J. Krause, R. James, G. D. Ruxton, N. R. Franks, Collective Memory and Spatial Sorting in Animal Groups. *Journal of Theoretical Biology* **218**, 1–11 (2002).

48. C. W. Reynolds, Flocks, herds and schools: A distributed behavioral model in *Proceedings of the 14th Annual Conference on Computer Graphics and Interactive Techniques*, SIGGRAPH '87., (Association for Computing Machinery, 1987), pp. 25–34.

49. T. Vicsek, A. Czirók, E. Ben-Jacob, I. Cohen, O. Shochet, Novel Type of Phase Transition in a System of Self-Driven Particles. *Phys. Rev. Lett.* **75**, 1226–1229 (1995).

50. C. C. Ioannou, M. Singh, I. D. Couzin, Potential Leaders Trade Off Goal-Oriented and Socially Oriented Behavior in Mobile Animal Groups. *The American Naturalist* **186**, 284–293 (2015).

51. A. Perna, *et al.*, Individual Rules for Trail Pattern Formation in Argentine Ants (Linepithema humile). *PLOS Computational Biology* **8**, e1002592 (2012).

52. I. Pinkoviezky, I. D. Couzin, N. S. Gov, Collective conflict resolution in groups on the move. *Physical Review E* **97** (2018).

53. S.-I. Amari, Homogeneous nets of neuron-like elements. *Biol. Cybernetics* **17**, 211–220 (1975).

54. S. Amari, Dynamics of pattern formation in lateral-inhibition type neural fields. *Biol. Cybern.* **27**, 77–87 (1977).

55. K. S. Kakaria, B. L. de Bivort, Ring Attractor Dynamics Emerge from a Spiking Model of the Entire Protocerebral Bridge. *Front. Behav. Neurosci.* **0** (2017).

56. L. Peliti, *Statistical Mechanics in a Nutshell* (Princeton University Press, 2011) (July 27, 2021).

57. J. J. Hopfield, Neural networks and physical systems with emergent collective computational abilities. *PNAS* **79**, 2554–2558 (1982).

58. K. G. Wilson, The renormalization group and critical phenomena. *Rev. Mod. Phys.* **55**, 583–600 (1983).

59. E. Schneidman, M. J. Berry, R. Segev, W. Bialek, Weak pairwise correlations imply strongly correlated network states in a neural population. *Nature* **440**, 1007–1012 (2006).

60. S. Takagi, R. Benton, Animal Behavior: A Neural Basis of Individuality. *Current Biology* **30**, R710–R712 (2020).

Materials and Methods

We construct a simple, spatially-explicit model of neural decision-making to study how the brain reduces choice in the presence of numerous spatial options (adapted from (52)). Theoretical predictions obtained were then tested experimentally by exposing invertebrate (fruit flies and desert locusts) and vertebrate systems (zebrafish) to spatial choice tests in virtual reality. To identify unifying principles of spatiotemporal computation across scales of biological organisation, we also reproduce the obtained decision-making patterns with an established model of collective decision-making in animal groups.

Neural decision-making model. We construct a computational model of neural decision-making that takes in a representation of directions to the different targets as input, and outputs a collective vectorial representation of the agent's future velocity (adapted from (52)). This provides us explicit predictions for animal trajectories, allows us to determine which target is reached in each realization of the simulation, and facilitates direct comparison with experimental tests. Our model is within the class of widely-employed neural ring-attractor models (see SI Appendix), which like neural field models (53, 54), and attractor network models more generally (15, 16, 55), consider the collective firing activity of the neurons, or the firing rate, as opposed to the microscopic state of each firing neuron.

In our model, the brain is composed of individual components, called "spins", that, collectively, as a "spin system", represent neural activity. Spin systems, which have been long-studied in physics due to their ability to give insight into a wide range of collective phenomena, from magnetic to quantum systems (56), were first introduced in the study of neurobiology by

Hopfield in a landmark paper (57) that provided considerable insights into principles underlying unsupervised learning and associative memory. In its simplest (and most common) formulation, as in Hopfield networks, a spin system is comprised of entities, spins, that can each be in state 0 or 1, or in the terminology of physics either 'up' or 'down'. Spin systems have consistently provided deep insights into complex collective phenomena, from spin and molecular systems, to neural systems, undergoing phase transitions (58, 59) (see SI Appendix for details and discussion).

Here, the animal's brain is characterized by a system of N spins. Each spin i encodes direction to one of the presented goals $\hat{p}_i$, and exists in one of two states: $\sigma_i=0$ or $\sigma_i=1$. We do not imply that a spin is equivalent to a neuron, but rather, as we show via a mathematical derivation, that the collective properties of interacting spins in our model is equivalent to the firing rate in the neural ring attractor model (see SI Appendix for details). Consequently, we refer to the individual components with which we model our system as "spins", and "neural activity" as a term to represent this "firing rate" equivalent. The energy of the system (for any given configuration) is given by its Hamiltonian, H.

$$H = -\frac{k}{N}\sum_{i\neq j} J_{ij}\sigma_i\sigma_j$$

where, k is the number of options available to the individual and J_{ij} is the interaction strength between neurons i and j. Here, J_{ij} is given by

$$J_{ij} = \cos\left(\pi\left(\frac{|\theta_{ij}|}{\pi}\right)^{\nu}\right)$$

where, θ_{ij} is the angle between preferred directions of neurons i and j, and ν represents the neural tuning parameter. For $\nu = 1$, the interactions become "cosine-shaped" $J_{ij} = \cos(\theta_{ij})$,

554 and the network has a Euclidean representation of space (Fig. S1). For $\nu < 1$, the network has
555 more local excitation and encodes space in a non-Euclidean manner (Fig. S1). System
556 dynamics are implemented by energy minimization using the Metropolis-Hastings algorithm
557 (similar to other Ising spin models) and the agent then moves with a velocity $\vec{V}$ determined by
558 the normalized sum of goal vectors $\hat{p}_i$ of all active neurons.

559 $$\vec{V} = \frac{v_0}{N} \sum_{i=1}^{N} \hat{p}_i \, \sigma_i$$

560 where v_0 is the proportionality constant. The goal vector $\hat{p}_i$ now points from the agent's
561 updated location to the neuron's preferred goal with directional noise chosen from a circularly
562 wrapped Gaussian distribution centered at 0 with a standard deviation σ_e. As in the mean-field
563 approximation of the model, the timescale of movement (defined by the typical time to reach
564 the target) in the numerical simulations was set to be much greater than the timescale of neural
565 firing (the typical time between two consecutive changes in the neural states σ_i).
566
567 **Collective decision-making model.** We reproduce results from our neural decision-making
568 model in a model that describes spatial decision-making at a different scale of biological
569 organization (refer (40) for methodological details). To highlight the features that are key to
570 producing the observed bifurcation patterns, we run simulations with and without feedback on
571 the strength of goal-orientedness of individuals.
572
573 **Fly virtual reality experiments.** All experiments were conducted on 3- to 5-day old female
574 wild-type CS strain *Drosophila melanogaster* raised at 26℃ on a 12 hr light, 12 hr dark cycle.
575 Experiments were conducted in a flyVR setup procured from loopbio GmbH. 60 tethered
576 *Drosophila melanogaster* were exposed to either a two-choice or a three-choice decision task
577 (30 and 30 individuals, respectively) in the virtual reality environment. Each experimental trial

lasted 15 min where flies were exposed to five sets of stimuli—three experimental sets and two control sets. The experimental stimuli sets consisted of two or three black cylinders (depending on the experimental condition) that were presented to the animal in an otherwise white environment. A control stimulus with a single pillar was presented before and after the experimental conditions. We rotated all trajectories such that the $x-$axis points from the origin, to the centre of mass of the targets. To visualise trajectories in the various experimental conditions, we created time-normalised (proportion of maximum across a sliding time window) density maps. We then folded the data about the line of symmetry, $y = 0$ and applied a density threshold to the time-normalised density map. A piecewise phase transition function was then fit to quantify the bifurcation.

$$y = \begin{cases} 0 & x \leq x_c \\ A|x - x_c|^{\alpha} & x > x_c \end{cases}$$

where x_c is the critical point, α is the critical exponent, and A is the proportionality constant. We also performed randomisation tests for each bifurcation where we conducted the exact fit procedure described above to data where the trajectories were randomised by keeping the x-coordinates, and swapping the y-coordinates with values from other random events. Randomizations show that the resultant fit to our experimental data were highly significant ($p < 0.01$ for binary choice and $p < 10^{-4}$ for the three-choice case).

Based on the amount of time it took flies to reach one of the available targets, we also classified individual fly tracks into one of two categories—direct tracks and non-direct tracks (60) (see Fig. S11A,H for details). In our model, the direct tracks were also accounted for by varying the directional tuning of spins. A high neural tuning (low ν) results in more directed tracks (Fig. S14).

Locust virtual reality experiments. All experiments were conducted on 156 instar 5 desert locusts (*Schistocerca gregaria*; 57 individuals for two-choice and 99 individuals for three-choice experiments, respectively) raised in the Animal Research Facility of the University of Konstanz. Based on our filtering criteria, 122 out of the 156 locusts were used in our analyses. Experiments were conducted in a locustVR setup procured from loopbio GmbH (27). The experimental procedure was identical to the one described above for flies, except now, each experimental trial lasted 48 min—three experimental sets (12 min each) and two control sets (6 min each). Analyzing bifurcations in locust trajectories using the same methods described above showed that the resultant bifurcations fit to our experimental data were highly significant ($p < 0.01$ for binary choice and $p < 10^{-4}$ for the three-choice case).

Similar to the flies, the locust trajectories were also classified as direct, or non-direct tracks. However, because the locustVR system allowed the animals to stop and reconsider movement during the decision-making process, we added an additional category to classification of individual locust tracks *viz.* the wandering tracks (see Fig. S12A,J for details).

Fish virtual reality experiments. All experiments were conducted on 1 cm ± 0.1 cm long zebrafish (*Danio rerio*) of age 24 to 26 days post-fertilisation raised in a room at 28 ℃ on a 16 hr light, 8 hr dark cycle. 440 fish were tested in total. Of these, 198 fish were exposed to decision-making with two virtual targets, 39 fish were exposed to decision-making with three equidistant virtual targets, and 50 fish were exposed to decision-making with three targets in asymmetric geometry (see SI Appendix for more details). Experiments were conducted in a fishVR setup procured from loopbio GmbH (refer (27) for details). Once a fish was introduced in the arena, it was given 20 min to acclimatize to the environment. This was followed by a 10 min control where it was presented a single virtual conspecific circling the arena in a circle of

627 radius 8 cm. After this, for experiments in symmetric geometries, the real fish was exposed to
628 choice experiments that lasted 90 min with the virtual fish initialized with random lateral
629 distances between them and random swim direction. To visualize the bifurcations, we
630 normalized (proportion of maximum) and stacked the marginal distributions along the direction
631 of the virtual fish's motion for various lateral distances. For experiments in asymmetric
632 geometries, the real fish was exposed to choice experiments where distance between the center
633 virtual fish and its closer neighbor was 0.03 m and its distance to the other neighbor was 0.09
634 m (Fig. 4). All experiments were conducted in accordance with the animal ethics permit
635 approved by Regierungspräsidium Freiburg, G-17/170.
636
637 **Acknowledgements.** We thank all members of the Department of Collective Behaviour who
638 assisted with the project: Renaud Bastien for modelling discussions and help setting up the VR
639 experiments, Guy Amichay for providing control data of two real fish swimming together, and
640 Paul Szyszka for showing V.H.S. how to tether flies. We thank the 'Itai Cohen Lab' for the
641 fruit fly image used in Fig. \ref{fig:insects}, Jitin Thomas for help with visualizations in Unity
642 and Andreas Poehlmann, John Stowers and Max Hofbauer from loopbio GmbH for technical
643 support with the VR systems. V.H.S., L.L., B.R.S. and I.D.C. are also grateful to the animal
644 care at the University of Konstanz including Christine Bauer, Jayme Weglarski and Dominique
645 Leo for help in conducting the experiments. They also acknowledge the efforts of the scientific
646 and technical staff at the University of Konstanz including Michael Mende, Markus Miller,
647 Mäggi Hieber Ruiz and Daniel Piechowski. V.H.S. acknowledges the International Max Planck
648 Research School (IMPRS) for Organismal Biology for the graduate school community and
649 access to courses and resources. I.D.C. acknowledges support from the NSF (IOS-1355061),
650 the Office of Naval Research grant (ONR, N00014-19-1-2556), the Struktur- und
651 Innovationsfonds für die Forschung of the State of Baden-Württemberg, the Deutsche

652 Forschungsgemeinschaft (DFG, German Research Foundation) under Germany's Excellence
653 Strategy-EXC 2117-422037984 and the Max Planck Society. N.S.G. is the incumbent of the
654 Lee and William Abramowitz Professorial Chair of Biophysics and acknowledges support by
655 the Minerva Foundation (grant no. 712601). M.N acknowledges support from the Eötvös
656 Loránd Research Network (a grant to the MTA-ELTE 'Lendület' Collective Behaviour
657 Research Group, grant number 95152, and MTA-ELTE Statistical and Biological Research
658 Group) and Eötvös Loránd University. Additionally, all authors thank two anonymous referees
659 for their constructive comments during the review process.

660

661 **Author contributions.** V.H.S. and I.D.C. designed the study; V.H.S., D.G., T.S., N.S.G. and
662 I.D.C. constructed the model; D.G. and N.S.G. constructed the mean-field approximation;
663 V.H.S. and I.D.C. designed the fly experiments; V.H.S. conducted these experiments and
664 analyzed the data with L.L. and M.N.; V.H.S., B.R.S. and I.D.C. designed the locust
665 experiments; B.R.S. conducted these experiments and V.H.S. analyzed the data with M.N.;
666 L.L. and I.D.C. designed the fish experiments; L.L. conducted these experiments and analyzed
667 this data with V.H.S. and M.N.; V.H.S. and I.D.C. drafted the manuscript with significant
668 contributions from all authors.

669

670 **Competing interests.** The authors declare that they have no competing interests.

671 **Figures.**

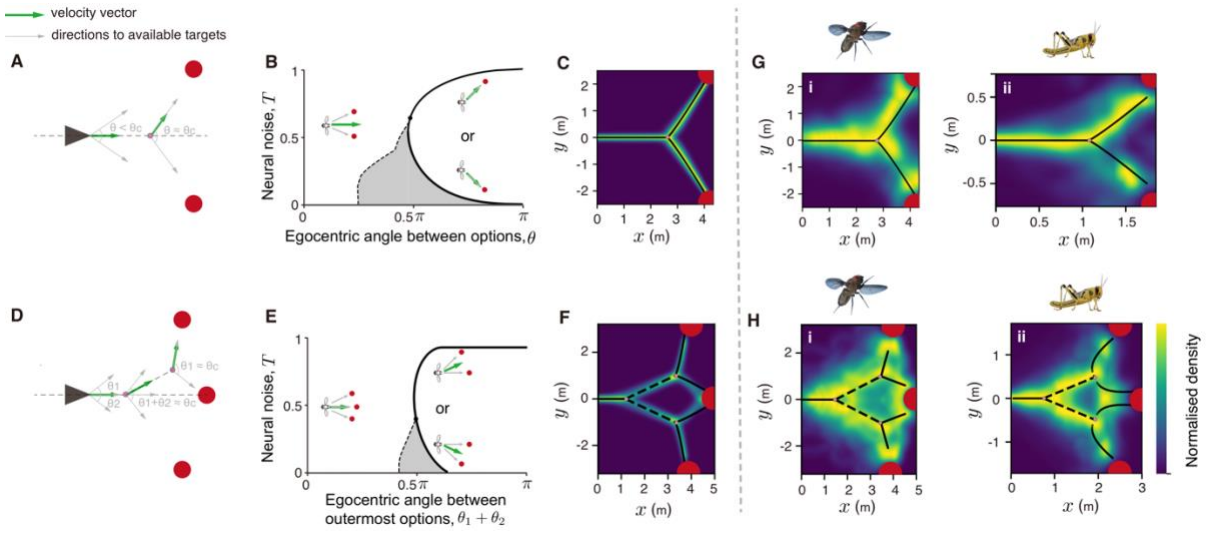

672

673 **Fig. 1.** Geometrical principles of two-choice and three-choice decision-making. (A) Schematic
674 of the binary decision-making experiments. This simplified representation shows that a sharp
675 transition in the animal's direction of travel is expected near a critical angle, θ_c. (B) A phase
676 diagram describing the 'critical' transition exhibited while moving from compromise to
677 decision between two options in space. The shaded area (also in E) represents the region in
678 parameter space where both the compromise, and the decision solutions exist. (C) Density plot
679 showing trajectories predicted by the neural model in a two-choice context. The axes represent
680 $x-$ and $y-$coordinates in Euclidean space. The black line (also in G) presents a piecewise
681 phase-transition function fit to the bifurcation. (D) Schematic of three-choice decision-making
682 experiments, where the central target is on the angle bisector of the angle subtended by the
683 other two targets. (E) A phase diagram describing the first 'critical' transition when the
684 individual chooses among three options. Once the individual eliminates one of the outermost
685 targets, it can decide between the two remaining options, similar to the two-choice phase
686 diagram described in B. (F) Theoretical predictions for decision-making in a three-choice
687 context. The dashed line (also in H) is the bisector of the angle subtended by center target and
688 the corresponding side target on the first bifurcation point. See Table S1 for parameters used
689 in C and F. (G) and (H) Density plots from experiments conducted with flies and locusts

690 choosing among two and three options, respectively. Note that the density plots presented here
691 are for the non-direct tracks, which constitute the majority type of trajectory adopted by both
692 flies and locusts (Figs. S11 and S12). However, our conclusions do not differ if we use all,
693 unfiltered, data (Figs. S11G,N and S12I,R).
694

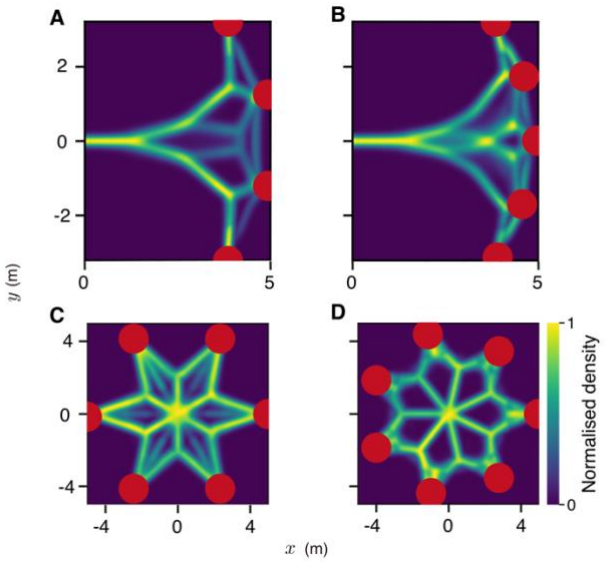

Fig. 2. Decision-making for a larger number of targets. Density plots of simulated trajectories for four- (A), five- (B), six- (C) and seven-choice (D) decision-making when targets are placed equidistant and equiangular from the agent. Thee axes represent $x-$ and $y-$coordinates in Euclidean space. Geometrical configurations are also varied to place the targets on the same side of the agent (A and B) or in radial symmetry (C and D). See Table S1 for parameters used in A–C. In D, all parameters used are identical except the system size $N = 70$.

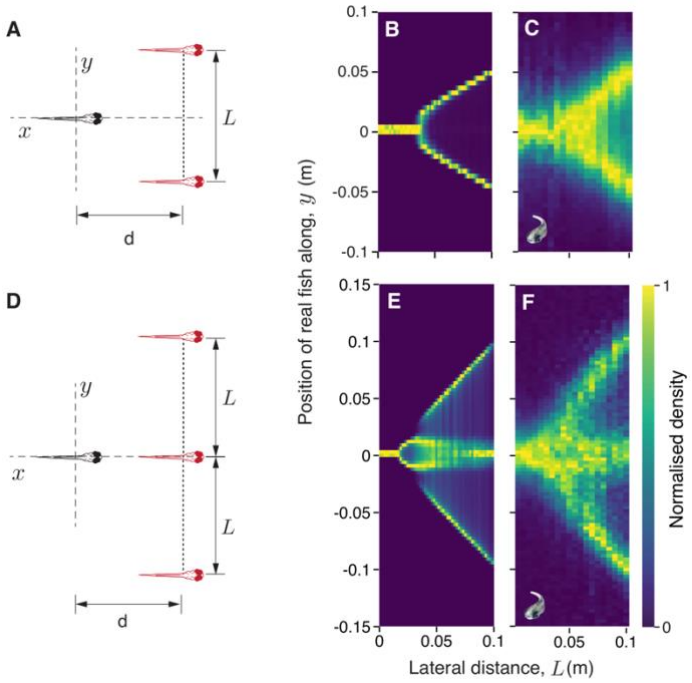

Fig. 3. Decision-making in a moving frame-of-reference. (A) Schematic of the two-choice decision-making experiments conducted with larval zebrafish. In these experiments (also in the three-choice experiments depicted in D), the virtual fish swim parallel to each other while maintaining a fixed lateral distance, *L* between them. We only consider data where the real fish swims behind the virtual fish, i.e., it follows the virtual fish (see SI Appendix and Fig. S15 for details). (B) Normalized probability distribution (proportion of maximum) of simulated positions of an agent following two moving targets, and corresponding experiments (C) conducted with larval zebrafish following two virtual conspecifics. (D) Schematic representation of the three-choice decision-making experiments. (E) Normalized probability distributions of simulated positions of an agent following three moving targets, and corresponding experiments (F) conducted with larval zebrafish following three virtual conspecifics. See Table S1 for model parameters used in B and E.

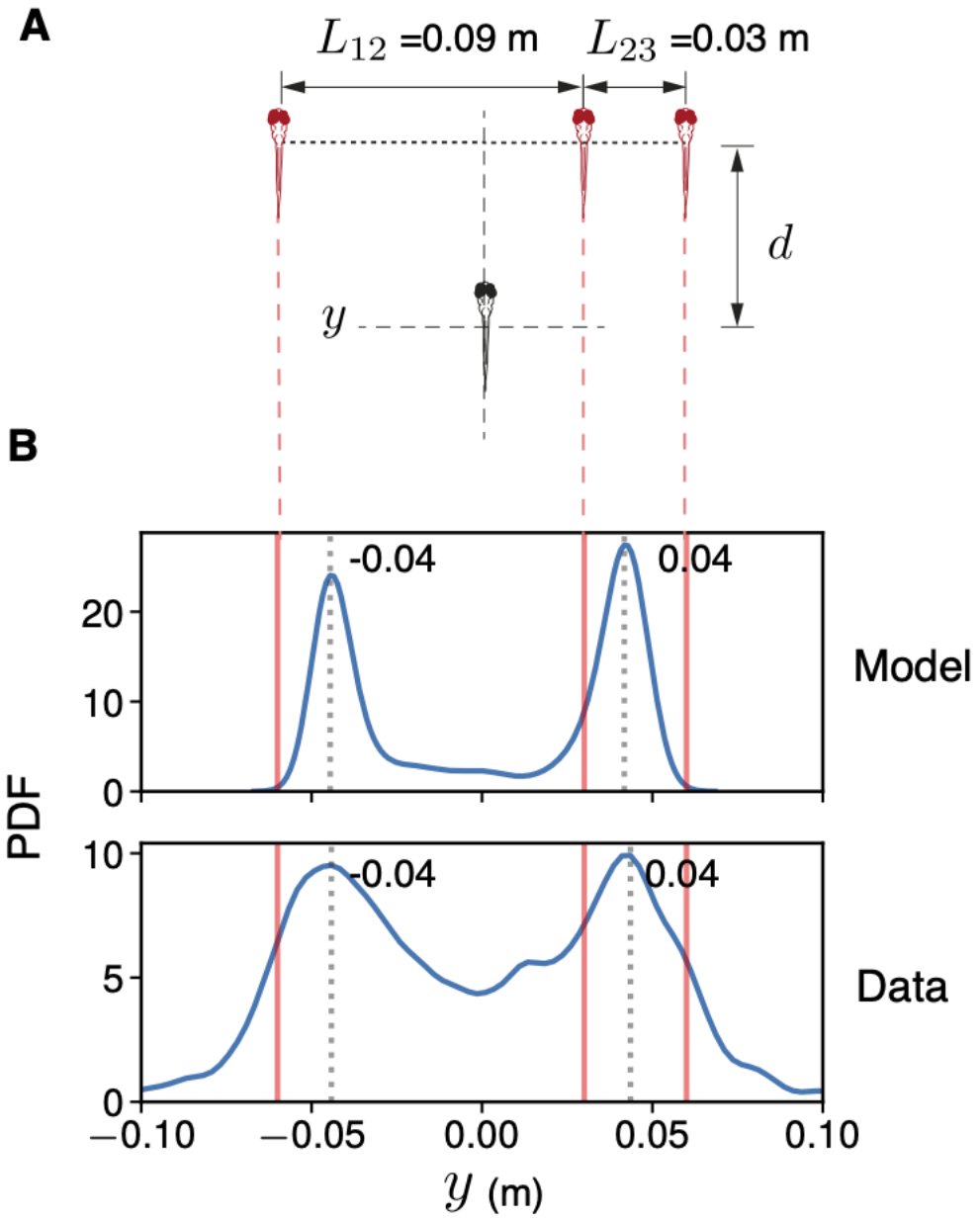

Fig. 4. Decision-making with the targets in an asymmetric geometry. (A) Schematic of the asymmetric choice test presented to larval zebrafish. In these experiments, the virtual fish swim parallel to each other while maintaining a fixed lateral distance, L between them. To create asymmetry in the geometry, the center fish swims closer to one of the side fish than the other ($L_{12} = 0.09$ m and $L_{23} = 0.03$ m). (B) The upper panel shows the probability density function of simulated positions of an agent following three moving targets in an asymmetric geometry corresponding to the experiments. The simulated agent occupies a position of $y =$

724 ± 0.04 m while following the targets ($\nu = 0.7$; $\sigma_\theta = 0.3$). The lower panel shows the
725 probability density function of the position of the real fish along the axis perpendicular to its
726 direction of motion. As predicted by our model, the real fish considers the two virtual
727 conspecifics closer to each other as a single target and adopts one of two positions behind the
728 virtual fish.
729

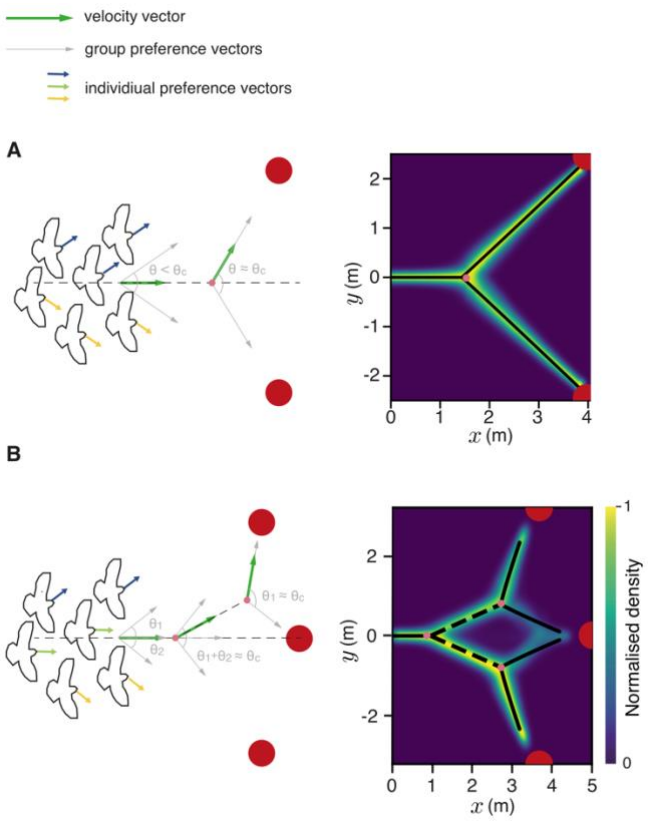

Fig. 5. Consensus decision-making in simulations of animal groups follow the same geometrical principles. Results for two- (A) and three-choice (B) decision-making in a model of animal collectives. The density plots show trajectories adopted by the centroid of the animal group for 500 replicate simulations where the groups don't split. The axes represent $x-$ and $y-$coordinates in Euclidean space. The black lines show a piecewise phase-transition function fit to the trajectories. For the three-choice case (B), the dashed line is the bisector of the angle subtended by center target and the corresponding side target on the first bifurcation point. See Table S2 for parameters used.